THE JOURNAL OF PHYSICAL CHEMISTRY LETTERS
A JOURNAL OF THE AMERICAN CHEMICAL SOCIETY

pubs.acs.org/JPCL Letter

Nonadiabatic Derivative Couplings through Multiple Franck–Condon Modes Dictate the Energy Gap Law for Near and Short-Wave Infrared Dye Molecules

Pablo Ramos, Hannah Friedman, Barry Y. Li, Cesar Garcia, Ellen Sletten, Justin R. Caram, and Seogjoo J. Jang*

Cite This: *J. Phys. Chem. Lett.* 2024, 15, 1802−1810 Read Online

ACCESS | Metrics & More | Article Recommendations | Supporting Information

ABSTRACT: Near infrared (NIR, 700−1000 nm) and short-wave infrared (SWIR, 1000−2000 nm) dye molecules exhibit significant nonradiative decay rates from the first singlet excited state to the ground state. While these trends can be empirically explained by a simple energy gap law, detailed mechanisms of nearly universal behavior have remained unsettled for many cases. Theoretical and experimental results for two representative NIR/SWIR dye molecules reported here clarify the key mechanism for the observed energy gap law behavior. It is shown that the first derivative nonadiabatic coupling terms serve as major coupling pathways for nonadiabatic decay processes from the first excited singlet state to the ground state for these NIR and SWIR dye molecules and that vibrational modes other than the highest frequency modes also make significant contributions to the rate. This assessment is corroborated by further theoretical comparison with possible alternative mechanisms of intersystem crossing to triplet states and also by comparison with experimental data for deuterated molecules.

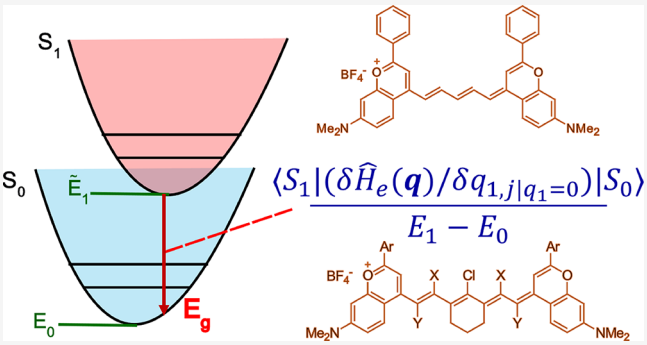

Despite the utility and reliability of the Born−Oppenheimer approximation[1,2] in general, nonadiabatic couplings between adiabatic potential energy surfaces can be significant in some cases, playing key roles for important quantum transfer and relaxation processes.[3−7] Well established examples include electron and proton transfer reactions and internal conversion between excited electronic states of comparable energies, for which various theoretical and computational advances[4−15] have been made. On the other hand, the role of nonadiabatic derivative couplings (NDCs) as direct routes for nonradiative transitions from the first excited singlet state to the ground electronic state has long remained unsettled. A widely held view[16,17] is that such direct nonadiabatic transitions are insignificant due to large energy gaps between excited and ground states. Thus, many nonradiative decay processes are hypothesized to occur through dark forbidden states or via an activated crossing to special nonadiabatic coupling regions such as conical intersections. Indeed, there are many examples with solid experimental evidence for transitions through such indirect[4,5,18] or special routes,[4,5,19] for which advanced theoretical and computational approaches have also been developed.[4,5,20] However, for near-infrared (NIR) dye molecules with wavelengths in the range of 700−1000 nm and short-wave infrared (SWIR) dye molecules in the range of 1000−2000 nm, direct nonadiabatic transitions through NDC from the first excited state to the ground state can play a significant role due to relatively small energy gaps and thus need to be examined more thoroughly.

Indeed, a recent work[21] by Friedman et al. reported fairly universal energy gap law[22,23] behavior of nonradiative decay rates for a broad class of NIR and SWIR dye molecules. Similar observation was reported more recently for different kinds of NIR dye molecules based on single molecule spectroscopy as well.[24] The observed experimental trends[21,24] suggest simple direct nonadiabatic transitions through NDC terms as major routes for nonradiative decays, which however have not been demonstrated clearly by any theoretical calculations yet. Given the growing importance of NIR and SWIR chromophores in biological imaging applications,[25−28] quantitative understanding of the role of NDCs on lifetimes of excited states also has significant implications and applications. The present Letter

Received: September 18, 2023
Revised: January 30, 2024
Accepted: January 31, 2024
Published: February 8, 2024

Downloaded via UNIV OF CALIFORNIA LOS ANGELES on August 12, 2024 at 01:50:02 (UTC).
See https://pubs.acs.org/sharingguidelines for options on how to legitimately share published articles.

ACS Publications © 2024 American Chemical Society

https://doi.org/10.1021/acs.jpclett.3c02629
J. Phys. Chem. Lett. 2024, 15, 1802−1810

elucidates this issue through detailed theoretical modeling of experimental lineshapes and nonradiative rates.

As representative cases, we here report comparative computational and experimental studies of two similar dye molecules, 7-dimethylamino flavylium pentamethine (Flav5) and 7-dimethylamino flavylium heptamethine (Flav7), and some deuterated forms of the latter molecule synthesized recently (see the Supporting Information (SI) for experimental details). Flav5 and Flav7 are NIR/SWIR dye molecules with similar structural motifs (see Figure 1), but their experimental nonradiative decay rates determined in dichloromethane (DCM) solvent, 3.2 ns^{-1} (Flav5) and 14.8 ns^{-1} (Flav7), are different by about a factor of 5.

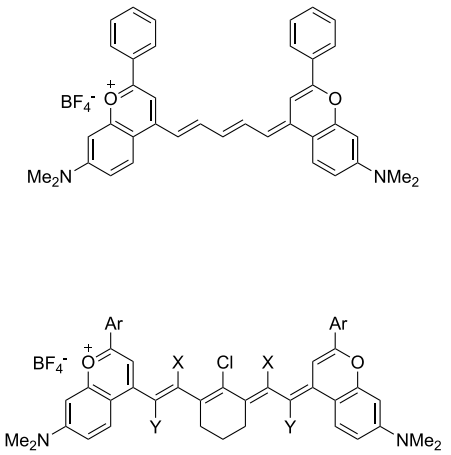

Figure 1. Comparison of the two organic dye molecules Flav5 (top) and Flav7 (lower panel). For the latter, X represents positions of hydrogen atoms being deuterated and Y represents those for which 30% of hydrogen atoms are deuterated. Flav7 with all hydrogen atoms in the aryl rings deuterated are also considered.

As computational methods for obtaining our theoretical data, we here employ the density functional theory (DFT)[29−31] and time dependent DFT (TD-DFT)[29,32,33] methods with the CAM-B3LYP functional,[34] which has been tested broadly and is known to produce fairly accurate values of reorganization energies[35] and Huang−Rhys (HR) factors.[36] Our choice is also supported by a recent comprehensive study[37] showing that CAM-B3LYP is one of the best functionals available for calculating excited state properties although it sometimes overestimates excitation energies.

For each molecule, we conducted optimization of the ground electronic state (S_0) structure, in the presence of a counterion, BF_4^-, employing the DFT method[29−31] with the CAM-B3LYP functional[34] and the 6-311+G basis set. Using the optimized structure of S_0 as the initial guess, we also optimized the structure of the excited state (S_1) for each molecule using the TD-DFT method[29,32,33] and using the same functional and basis set.

The theoretical $S_0 \rightarrow S_1$ transition energies for the optimized structure of S_0 in vacuum calculated by the TD-DFT method (with default value of tuning parameter ω = 0.33 bohr^{-}1 for CAM-B3LYP functional) are 2.2801 eV for Flav5 and 2.0599 eV for Flav7. We find that these are significantly larger than experimental vertical absorption energies (in DCM), which we estimated from line shape modeling as will be described later and are 1.440 eV for Flav 5 and 1.207 eV for Flav7. Similarly, calculated values of vertical $S_1 \rightarrow S_0$ transition energies in vacuum for the optimized structure of S_1 are 2.0935 eV for Flav5 and 1.8835 eV for Flav7, which are also larger than experimental solution phase values of 1.378 eV for Flav5 and 1.177 eV for Flav7. For better understanding of the sources of the discrepancies, we also conducted calculations employing other functionals and considering solvation effects at the continuum level. The SI provides these values and discusses their implications. Outcomes of these calculations suggest that

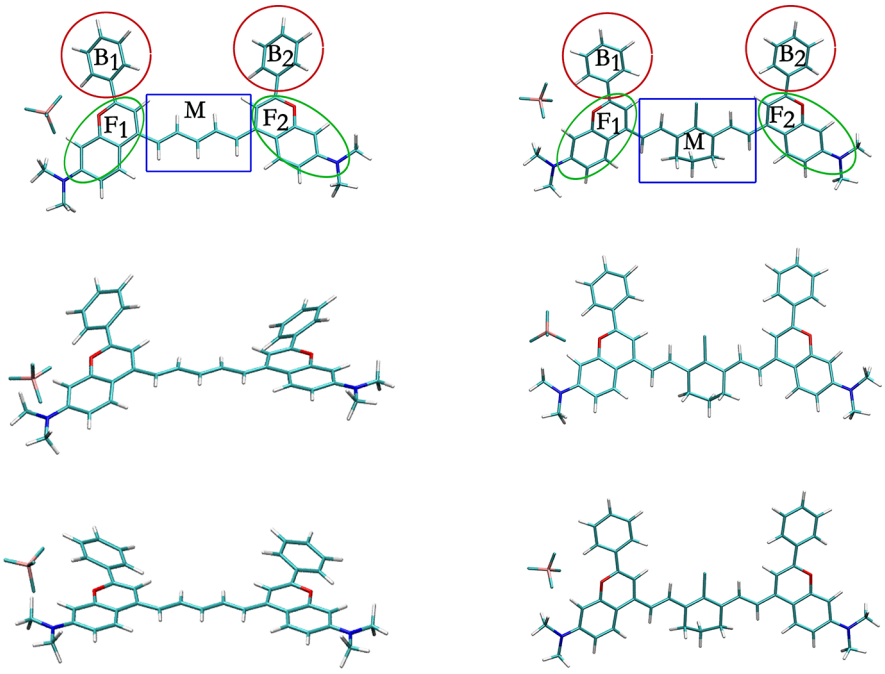

Figure 2. Comparison of the structures of the Flav5 (left column) and Flav7 (right column) dye molecules. The top row provides chemical structures indicating different sections with different labels. The middle row shows optimized structures for the S_0 state, and the bottom row shows those for the S_1 state.

https://doi.org/10.1021/acs.jpclett.3c02629
J. Phys. Chem. Lett. 2024, 15, 1802−1810

SCAN functional[38] in fact produces excitation energies in better agreements with experimental ones. However, they are still significantly larger than the experimental excitation energies, and the SCAN functional has not yet been tested well enough for calculating FC factors and NDC terms. In fact, for SCAN, including solvent effect results in blue shift of excitation energies (see Table S2). Our preliminary calculation of line shape based on SCAN functional also suggests its performance for calculating FC factors is not reliable, which is consistent with a recent study in favor of CAM-B3LYP over SCAN.[37] Thus, for our theoretical modeling in this work, we employ all computational data obtained from the CAM-B3LYP functional except for the excitation energies for which we use values obtained from experimental data. The validity of this approach is supported by good agreements between theoretical and experimental absorption lineshapes as will become clear.

In Figure 2, the optimized structures for both dye molecules are shown. Structures shown at the top include labels for different parts of the molecule, which are used for providing more detailed analyses below. For each molecule, the structure of S_0 state is asymmetric and the F1 flavylium heterocycle is tilted with respect to the molecular plane, which is defined as a plane that contains the M section maximally. On the other hand, the F2 heterocycle is nearly coplanar with the molecular plane. The angle between the F1 heterocycle and the molecular plane is 18.0° for Flav5 and 26.0° for Flav7. The B1 ring has an angle of 20.4° and 25.0° for Flav5 and Flav7, respectively, and the angle of the B2 phenyl group is about 30.0° with respect to the molecular plane in both dyes, although they are in opposite directions. Thus, for the S_0 state, the major structural difference between the two dye molecules lies in detailed orientational features of ring parts. On the other hand, for the S_1 states, structures are similar and more symmetric, with B1 and B2 heterocycles at about 17° with respect to the molecular plane. Both the F1 and F2 parts are nearly coplanar with the M section, which is flat for Flav5 but is concave for Flav7 due to the presence of bridging sp^3 carbons in the 7-methine M group.

For theoretical calculation of absorption and emission lineshapes, we evaluated HR factors[39] for both the vertical $S_0 \rightarrow S_1$ transition at the optimized structure of S_0 and also those for the $S_1 \rightarrow S_0$ transition at the optimized structure of S_1. For each molecule, there were clear differences between the two distributions of HR factors at the S_0 and S_1 states, which reflects the presence of significant anharmonic effects. This is understandable considering the significant differences in the optimized structures for the S_0 and S_1 states as can be seen from Figure 2. We account for such anharmonic contributions by introducing two different baths of harmonic oscillators defined differently depending on the structure of the initial state, as described below. Before providing a more detailed description of models, we find it useful to clarify notations we adopt in this work. S_0 and S_1 denote the whole set of the ground and the first excited adiabatic electronic states, respectively, parametrized by nuclear coordinates. On the other hand, we introduce two diabatic states based on crude adiabatic approximation, $|\tilde{S}_0\rangle$ and $|\tilde{S}_1\rangle$, which are determined at the optimized minimum energy nuclear coordinates of the S_0 surface. Similarly, we define another two diabatic states, $|S_0\rangle$ and $|\tilde{S}_1\rangle$, which are determined at the optimized minimum energy nuclear coordinates of the S_1 surface.

We assume that the molecular Hamiltonian near the structure optimized for the S_0 state of each molecule can be approximated by the following model:

$$\hat{H}_0 = \tilde{E}_0|\tilde{S}_0\rangle\langle\tilde{S}_0| + \left\{E_1 + \sum_n \hbar\omega_n g_{n,10}(\hat{b}_n + \hat{b}_n^\dagger)\right\}|S_1\rangle\langle S_1| + \sum_n \hbar\omega_n\left(\hat{b}_n^\dagger\hat{b}_n + \frac{1}{2}\right) \quad (1)$$

where $\tilde{E}_0$ and E_1 are electronic energies of S_0 and S_1 states, respectively, for a fully optimized structure of the molecule in the S_0 state, and $\hat{b}_n$ and $\hat{b}_n^\dagger$ represent lowering and raising operators for each harmonic oscillator normal mode of molecular vibrations calculated for the optimized structure of the S_0 state (see Figure 3 for a schematic illustration). The coupling constant $g_{n,10}$ represents the extent of displacement of the nth normal mode upon excitation, the square of which is the corresponding HR factor for the $S_0 \rightarrow S_1$ transition near the structure optimized for the S_0 state. Note that the tilde symbol in $\tilde{E}_0$ indicates that it is the energy for the fully relaxed (optimized) structure of the S_0 state, in contrast to E_1. Thus, $E_1 - \tilde{E}_0$ is the vertical excitation energy for the $S_0 \rightarrow S_1$ transition at the optimized structure of S_0.

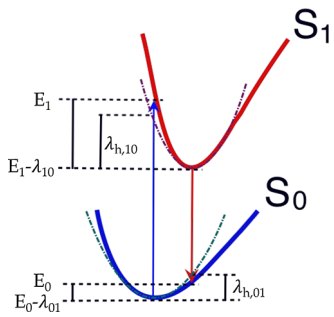

Figure 3. Schematic of adiabatic potential energy surfaces for S_0 (lower blue line) and S_1 (upper red line) electronic states, which are in general anharmonic and relevant energies. λ_{10} is the reorganization energy in the S_1 state from the minimum energy structure of S_0 to the optimized structure of S_1, and λ_{01} is the reorganization energy in the S_0 state from the minimum energy structure of S_1 to the optimized structure of S_0. Note that $\tilde{E}_0 = E_0 - \lambda_{01}$ and $\tilde{E}_1 = E_1 - \lambda_{10}$. Reorganization energies within the harmonic approximation $\lambda_{h,10}$ and $\lambda_{h,01}$ are also shown (see text for more detailed explanation).

On the other hand, for the structures optimized at the S_1 state, we assume that the molecular Hamiltonian can be approximated by the following model:

$$\hat{H}_1 = \left(E_0 + \sum_n \hbar\omega_n g_{n,01}(\hat{b}_n + \hat{b}_n^\dagger)\right)|S_0\rangle\langle S_0| + \tilde{E}_1|\tilde{S}_1\rangle\langle\tilde{S}_1| + \sum_n \hbar\omega_n\left(\hat{b}_n^\dagger\hat{b}_n + \frac{1}{2}\right) \quad (2)$$

where E_0 and $\tilde{E}_1$ are electronic energies of S_0 and S_1 states respectively for a fully optimized structure of the molecule in the S_1 state, and $\hat{b}_n$ and $\hat{b}_n^\dagger$ represent lowering and raising operators for each harmonic oscillator normal mode of molecular vibrations calculated for the optimized structure of the S_1 state (see Figure 3 for a schematic illustration.). The coupling constant $g_{n,01}$ represents the extent of displacement of the nth normal mode, the square of which is the corresponding HR factor, for the $S_1 \rightarrow S_0$ transition near the structure optimized for the S_1 state.

https://doi.org/10.1021/acs.jpclett.3c02629
J. Phys. Chem. Lett. 2024, 15, 1802−1810

Note that $\tilde{E}_1 = E_1 - \lambda_{10}$ and $E_0 = \tilde{E}_0 + \lambda_{01}$ (see Figure 3). Thus, λ_{10} is the reorganization energy in the S_1 electronic state for the structural change from the minimum S_0 energy to that of S_1. On the other hand, λ_{01} is the reorganization energy in the S_0 electronic state for the structural change from that of the minimum S_1 energy to that of S_0. Thus, $\tilde{E}_1 - E_0$ is the vertical emission energy for the transition to S_0 from the fully relaxed S_1 state. Note that λ_{10} and λ_{01} include all of the anharmonic effects of conformational changes as well as harmonic contributions of the molecular vibrations. Thus, they are different from those based on the harmonic oscillator bath modes. Note also that the oscillator modes in eqs 1 and 2 are different but are denoted with the same labels.

Let us define the following bath spectral densities:

$$\mathcal{J}_{ij}(\omega) = \pi\hbar \sum_n \delta(\omega - \omega_n)\omega_n^2 g_{n,ij}^2 \tag{3}$$

where $i,j = 1,0$ (for eq 1) or 0,1 (for eq 2), and the corresponding real and imaginary parts of the line shape function:

$$G_{R,ij}(t) = \frac{1}{\pi\hbar}\int_0^\infty d\omega \frac{\mathcal{J}_{ij}(\omega)}{\omega^2}\coth\left(\frac{\hbar\omega}{2k_BT}\right) \times (1 - \cos(\omega t))$$

$$G_{I,ij}(t) = \frac{1}{\pi\hbar}\int_0^\infty d\omega \frac{\mathcal{J}_{ij}(\omega)}{\omega^2}(\sin(\omega t) - \omega t) = \frac{1}{\pi\hbar}\int_0^\infty d\omega \frac{\mathcal{J}_{ij}(\omega)}{\omega^2}\sin(\omega t) - \frac{\lambda_{h,ij}}{\hbar}t \tag{5}$$

with $\lambda_{h,ij} = \hbar\sum_n \omega_n g_{n,ij}^2$. Note that $\lambda_{h,10}$ and $\lambda_{h,01}$ are harmonic approximations for $\lambda_{10} = E_1 - \tilde{E}_1$ and $\lambda_{01} = E_0 - \tilde{E}_0$, as indicated in Figure 3. Thus, $\lambda_{10} - \lambda_{h,10}$ represents contributions of anharmonicity in the S_1 surface, whereas $\lambda_{01} - \lambda_{h,01}$ represents that in the S_0 surface. In the simplest displaced harmonic oscillator model for which S_1 and S_0 are parabolic forms of the same curvature, $\lambda_{01} = \lambda_{10} = \lambda_{h,01} = \lambda_{h,10}$.

The normalized absorption line shape for $S_0 \to S_1$ transition, for the Hamiltonian of eq 1, based on the Fermi's golden rule (FGR) for interaction with radiation within the dipole approximation,[40] can be expressed as

$$I_{S_0\to S_1}(\omega) = \frac{1}{2\pi}\int_{-\infty}^{\infty} dt \exp\left\{i\left(\omega - \frac{(E_1 - \tilde{E}_0)}{\hbar}\right)t - G_{R,10}(t) - iG_{I,10}(t)\right\} \tag{6}$$

On the other hand, the normalized emission line shape for $S_1 \to S_0$ transition, for the Hamiltonian of eq 2, can be expressed as[40]

$$E_{S_1\to S_0}(\omega) = \frac{1}{2\pi}\int_{-\infty}^{\infty} dt \exp\left\{i\left(\omega - \frac{(\tilde{E}_1 - E_0)}{\hbar}\right)t - G_{R,01}(t) + iG_{I,01}(t)\right\} \tag{7}$$

For actual calculation of lineshapes, we employed a Lorentzian function for the delta function in eq 3. Thus, the following approximations were used.

$$\mathcal{J}_{ij}(\omega) \approx \hbar \sum_n \frac{\omega_n^2 g_{n,ij}^2 \sigma}{\sigma^2 + (\omega - \omega_n)^2} = 2\pi c\hbar \sum_n \frac{\tilde{\nu}_n^2 g_{n,ij}^2 \tilde{\nu}_\sigma}{\tilde{\nu}_\sigma^2 + (\tilde{\nu}_n - \tilde{\nu})^2} \tag{8}$$

where $\tilde{\nu} = \omega/(2\pi c)$, $\tilde{\nu}_n = \omega_n/(2\pi c)$, and $\tilde{\nu}\sigma = \sigma/(2\pi c)$. The choice of $\tilde{\nu}_\sigma$ can be made such that it is small enough to discern all different vibrational frequencies, and we found that the choice of $\tilde{\nu}_\sigma = 22\ \mathrm{cm}^{-1}$ reasonable. The resulting spectral densities calculated by the TD-DFT method with CAM-B3LYP functional are provided in Figures S1 and S2 in the SI.

Figure 4 compares theoretical absorption and emission lineshapes for Flav5 and Flav7 calculated according to eqs 6 and 7, respectively, with experimental lineshapes. The peak maxima of theoretical lineshapes were shifted uniformly to match experimental ones as indicated in the figure caption, but no other corrections were made. The resulting values of $E_1 - \tilde{E}_0$ and $\tilde{E}_1 - E_0$ determined in this manner are listed in Table 1. Theoretical values of reorganization energies and their harmonic approximations for both the ground and excited state energies are provided as well. Considering the simplicity of underlying models and the fact that solvation effects have not been

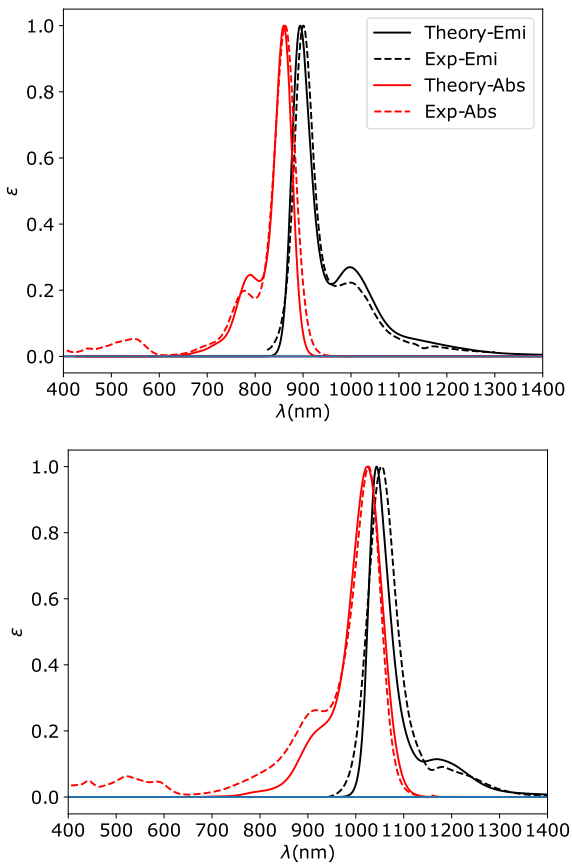

Figure 4. Absorption ($S_0 \to S_1$) and emission ($S_1 \to S_0$) lineshapes for Flav5 (upper) and Flav7 (lower). Experimental lineshapes in the solution phase are compared with theoretical lineshapes of isolated molecules, which were shifted to match the corresponding maxima of experimental spectra. For the absorption, the shifts were 1.423 eV for Flav5 and 1.191 eV for Flav7. For the emission, the shifts were 1.405 eV for Flav5 and 1.185 eV for Flav7. We also normalized heights with respect to those of their maxima.

https://doi.org/10.1021/acs.jpclett.3c02629
J. Phys. Chem. Lett. 2024, 15, 1802−1810

Table 1. Energy Gap Values Best Matching Peak Positions of Experimental Lineshapes for Flav 5 and Flav 7[a]

Dye	$E_1 - \tilde{E}_0$ (eV)	$\tilde{E}_1 - E_0$ (eV)	λ_{10} (eV)	$\lambda_{h,10}$ (eV)	λ_{01} (eV)	$\lambda_{h,10}$ (eV)
Flav5	1.440	1.378	0.817	0.455	0.630	0.349
Flav7	1.207	1.177	0.701	0.631	0.524	0.283

[a]Theoretical values of the reorganization energies are also shown. Note that $\lambda_{10} = E_1 - \tilde{E}_1$ and $\lambda_{01} = E_0 - \tilde{E}_0$.

included, the agreements are excellent. This suggests that major vibronic interactions are reasonably represented by normal modes of molecular vibrations, modeled as harmonic oscillators, and that contributions of solvents on details of lineshapes are minor. This good agreement also means that HR factors calculated by using the CAM-B3LYP functional are quite reliable. It is worth noting that small peaks around 500 nm in experimental absorption lineshapes correspond to excitations to higher electronic states, which are not included in our calculations. In addition, while other small disagreements between theoretical and experimental lineshapes could in principle be accounted for by inclusion of solvent effects, simple calculations based on polarizable continuum model turned out to worsen theoretical lineshapes compared to experimental ones (see the SI). Therefore, a more accurate solvation model is necessary for better quantitative agreement.

As can be seen from Figure 4, the absorption lineshape for each molecule has a prominent sideband followed by broad tail in the blue region. For Flav5, the major sideband is attributed to two groups of normal modes (see the SI for the depiction of major normal modes.). The first group corresponds to wagging motions of H atoms at 1,026 cm^{-1}, which are broadened by those of heavy atoms at around 675 cm^{-1}. The second group consists of the scissoring motion of heavy atoms at 1237 cm^{-1} and H atoms at 1242 cm^{-1} respectively. The broad tail region is due to the high energy modes and is related to the rocking motion of H atoms in the structure and the stretching motion of H atoms in the aliphatic chain. For Flav7, the major sideband is due to the wagging motion of the benzene ring carbons at 825 cm^{-1}, scissoring motion of H atoms at 1252 cm^{-1}, and the wagging motion of H atoms at 1509 cm^{-1}. The broad blue tail is also contributed by these wagging modes with the addition of the stretching motion of H atoms within the central parts of molecules. The stretching of the aliphatic chain at 2980 cm^{-1} and the stretching of H atoms in aromatic rings at 3150 cm^{-1} also make some contributions. Similar features appear in the respective emission lineshapes on the red side of major peaks. More detailed information on bath spectral densities and major vibrational modes can be found in the SI.

For the optimized structure in the S_1 state of each molecule, we calculated first NDC terms[41,42] in Cartesian coordinates, which were then projected onto different mass weighted normal modes of vibration. The resulting expression is as follows:

$$\mathrm{NDC}_j = \frac{|\langle \tilde{S}_1 | (\partial \hat{H}_e(\mathbf{q})/\partial q_{1,j}|_{\mathbf{q}_1=0}) | S_0 \rangle|}{\tilde{E}_1 - E_0} \tag{9}$$

where $q_{1,j}$ represents the jth mass-weighted normal mode in the S_1 state around its minimum energy structure. Detailed derivation of the above expression starting from full molecular Hamiltonian in the adiabatic basis[2,43] is provided in the SI.

In general, nonadiabatic couplings can be very different in different molecular conformations, especially when two energies are near degenerate. However, for the case of $S_1 \rightarrow S_0$ transition, where the two electronic states are far from degeneracy and there are no other states of comparable energies as considered here, it is most likely that the NDC values are fairly insensitive to the displacements from the minimum energy structure of the S_1 state. To examine this issue, we conducted additional calculations of NDC terms varying the values of nuclear coordinates, which indeed confirm our assumption and justify using the NDC values for the optimized structures of S_1 (see the SI and Figures S8−S11).

Under the same assumption, we also calculated the NDC terms for partially and fully deuterated Flav5 and Flav7 molecules. Figure 5 shows distributions of these projected

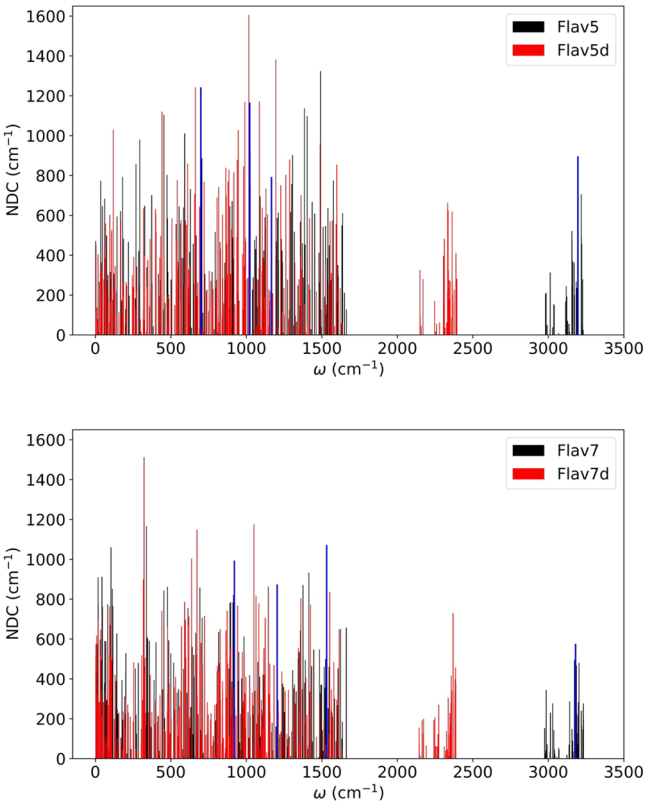

Figure 5. Nonadiabatic couplings projected on to each normal mode for Flav5 (upper panel) and Flav7 (lower panel). Black lines represent results for original molecules and red lines represent those for fully deuterated ones.

NDC terms for the original and fully deuterated molecules. Results in Figure 5 show broad distributions of NDC terms up to about 1,600 cm^{-1} and another well separated high frequency bands, which correspond to C−H (or C−D) stretching modes. It is interesting to note that the contributions of these high frequency modes are rather small compared with those due to broad low frequency modes. To examine the validity of our simple displaced harmonic oscillator models, we also calculated the Duschinsky rotation matrix[44,45] from the displacements of the nuclei in the normal modes. Results provided in the SI suggest that Duschinsky effects are not likely to affect the major conclusion of this work.

The transition due to NDC is intrinsically non-Condon type, because it involves nuclear momentum operators. On the other hand, the derivation of the energy gap is based on the FGR rate expression within the Condon approximation. Thus, we here

https://doi.org/10.1021/acs.jpclett.3c02629
J. Phys. Chem. Lett. 2024, 15, 1802−1810

introduce an effective coupling constant that accounts for the non-Condon effect in an average manner by using thermally averaged momentum as follows:

$$J_{eff} = \hbar \sum_{j=1}^{N_v} \mathrm{NDC}_j \left(\frac{\sum_{v_j=0}^{\infty} \langle p_{v_j}^{\,2} \rangle^{1/2} e^{-\hbar\omega_j(v_j+1/2)/(k_B T)}}{\sum_{v_j=0}^{\infty} e^{-\hbar\omega_j(v_j+1/2)/(k_B T)}} \right) \tag{10}$$

where NDC_j is given by eq 9 and $\langle p_{v_j}^2 \rangle^{1/2} = \sqrt{\hbar\omega_j\left(v_j + \frac{1}{2}\right)}$, the root-mean-square momentum of each vibrational mode with vibrational quantum number v_j. More detailed justification of the above expression and description of the calculation method are provided in SI. The resulting values of J_{eff} for the $|\tilde{S}_1\rangle \rightarrow |S_0\rangle$ of different cases are provided in Table 2. Note that in calculating these values we have used experimental values determined from emission spectra for $\tilde{E}_1 - E_0$ whereas all other values were obtained from TD-DFT calculations employing the CAM-B3LYP functional.

Table 2. Theoretical Data for the Effective Electronic Coupling J_{eff}, eq 10, and the Nonradiative FGR Rate, eq 12, for $S_1 \rightarrow S_0$ Transitions for Flav5, Flav5$_D$ (Fully Deuterated), Flav7, and Flav7$_D$ (Fully Deuterated), and Partially Deuterated Flav7 (with Different Subscripts Representing Parts of Deuteration)[a]

Dye	Theory ($S_1 \rightarrow S_0$)		
	J_{eff} (cm^{-1})	k_{nr} (ns^{-1})	k_{exp} (ns^{-1})
Flav5	425.3	1.041	3.2
	(424.8)	(0.812)	
Flav5$_D$	388.2	0.904	
	(388.1)	(0.600)	
Flav7	918.8	8.350	14.7
	(917.4)	(7.297)	
Flav7$_D$	756.8	6.081	
	(756.5)	(5.660)	
Flav7$_{mD2}$	596.0	5.133	14.1
Flav7$_{mD2.12}$	654.8	3.727	13.8
Flav7$_{ArD10}$	482.3	1.984	13.5

[a]Experimental nonradiative decay rates are also shown. For the calculation of theoretical rates, experimental values of the energy gap, as listed in Table 1, were used. Theoretical data for the hypothetical cases where the high frequency C−H (or C−D) stretching modes are turned off are also shown in parentheses.

For the calculation of nonradiative transition rate due to the effective electronic coupling J_{eff} given by eq 10, we use an effective two state model coupled to harmonic oscillator baths represented by the following Hamiltonian:

$$\hat{H}_{nr} = \tilde{E}_1 |\tilde{S}_1\rangle\langle\tilde{S}_1| + \left(E_0 + \sum_n \hbar\omega_n g_{n,01} (\hat{b}_n + \hat{b}_n^{\dagger}) \right) |S_0\rangle\langle S_0| + J_{eff}(|\tilde{S}_1\rangle\langle S_0| + |S_0\rangle\langle\tilde{S}_1|) + \sum_n \hbar\omega_n \left(\hat{b}_n^{\dagger}\hat{b}_n + \frac{1}{2} \right) \tag{11}$$

Note that the above model Hamiltonian is the same as that used for the emission line shape except that the two electronic states are now coupled by J_{eff}.

The FGR rate for the above model Hamiltonian is as follows:[40]

$$k_{FG} = \frac{J_{eff}^{\,2}}{\hbar^2} \int_{-\infty}^{\infty} dt \exp\left\{ \frac{i}{\hbar}(\tilde{E}_1 - E_0)t - G_{R,01}(t) - G_{I,01}(t) \right\} \tag{12}$$

where $G_{R,01}(t)$ and $G_{I,01}(t)$ are respectively defined by eqs 4 and 5 with $i = 0$ and $j = 1$.

Figure 6 shows calculated nonradiative rates for a range of energy gap values. The actual values of energy gaps, which are shown as vertical lines, are 1.378 eV for Flav5 and 1.177 eV for Flav7. These confirm that actual transitions indeed occur within ranges where the energy gap law behavior[22,23] is expected. In order to determine the contribution of the high frequency C−H or C−D stretching modes to these rates, we also calculated rates with the contributions of those modes to HR factors turned off. The resulting data are shown as red lines. Eliminating these high frequency contributions indeed reduces rates more significantly as the gap increases.

Table 2 shows values of theoretical rates determined from the actual experimental energy gap values (vertical lines) in Figure 6. Experimental nonradiative rates are also provided for comparison (see the SI for details on how these rates were determined). The theoretical values are smaller than experimental ones, which we attribute to contributions of Duschinsky rotation effects[46−50] and non-Condon effects that are not accounted for by our model Hamiltonian and rate expression. In particular, we expect that inclusion of explicit consideration of momentum non-Condon effects in NDC, for which closed form rate expression is possible,[51] can account for the significant portion of the discrepancy. Nonetheless, the theoretical trends agree well with experimental ones. For both original and fully deuterated molecules, we also determined rates for the hypothetical situation where high frequency C−H or (C−D) stretching modes do not contribute. The resulting theoretical values, which are shown in parentheses, clarify that the contributions of high frequency modes to the total NDCs and rates are relatively small for these cases.

In addition to fully deuterated cases, we also calculated rates with partial deuteration. The Flav7 molecules denoted with m.D2 and m.D2.12 are those where the deuteration takes place at the aliphatic hydrogen, whereas that with Ar.D10 has aromatic hydrogens deuterated. These changes result in a modest reduction of effective couplings and rates. This indicates that deuteration of hydrogen atoms, which affects both HR factors and the effective couplings mainly through frequency changes of normal modes, indeed makes some contributions to the rate but is not a determining factor. We find that these computational results are also consistent with experimental data (see Table 2).

In order to examine the possibility of alternative nonradiative decay processes through triplet states, we also determined first (T_1) and second (T_2) excited triplet states and calculated FGR rates for the following four possible transitions: $T_1 \rightarrow S_0$; $T_2 \rightarrow S_0$; $S_1 \rightarrow T_1$; and $S_1 \rightarrow T_2$. For the estimation of these rates, we used the spectral densities of normal modes determined for the S_1 state, spin−orbit coupling constants determined as detailed in the SI for the effective electronic coupling constant in eq 12. Figures S10 and S11 provide the dependence of these theoretical rates on the value of the energy gap between singlet and triplet states. Table S2 of the SI provides the corresponding theoretical values of the energy gap, effective coupling constants, and rates. These show that all of the singlet−triplet spin−orbit couplings are less than 1 cm^{-1} and that transition rates are less than 10^5 s^{-1}.

https://doi.org/10.1021/acs.jpclett.3c02629
J. Phys. Chem. Lett. 2024, 15, 1802−1810

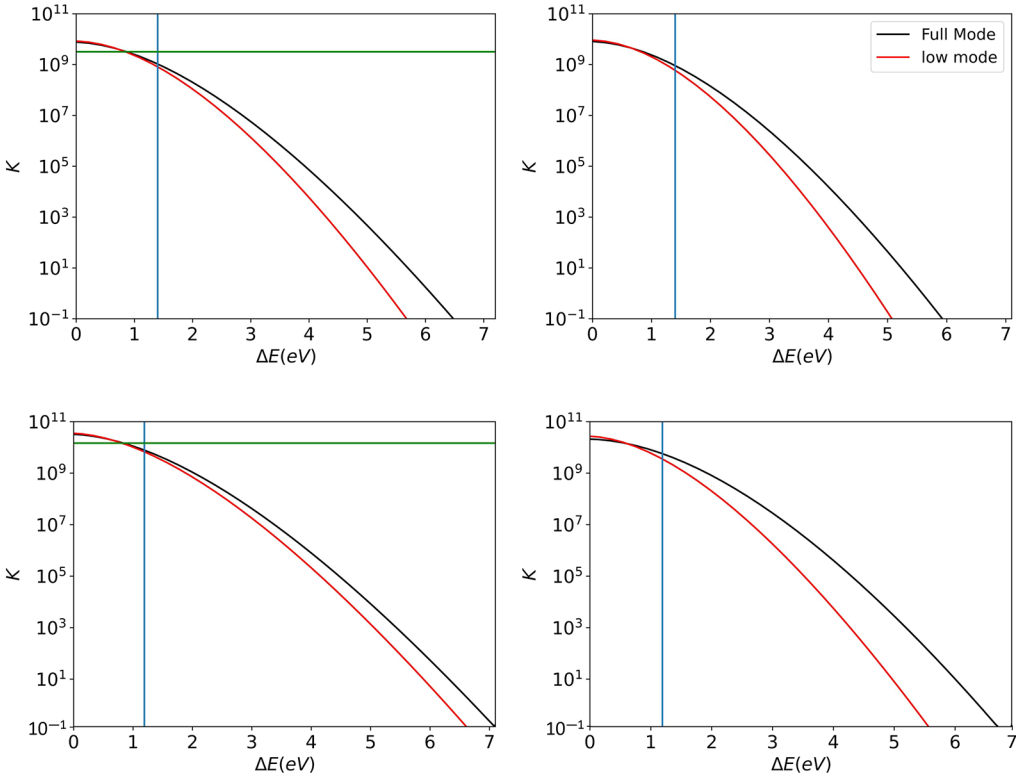

Figure 6. Nonadiabatic transition rates (in logarithmic scale) versus energy gap for the $S_1 \rightarrow S_0$ electronic transitions for both Flav5 (upper panel) and Flav7 (lower panel) dyes, where the vertical lines represent the experimental energy gap value between the two states, $\tilde{E}_1 - E_0$, which are 1.378 eV for Flav5 and 1.177 eV for Flav7. Rates versus the energy gap are shown for the original molecules (left) and deuterated (right) molecules. The experimental rates for the original molecules are shown as horizontal lines. Red curves represent transition rates calculated with the high energy vibrational modes nullified.

Although additional approximations were involved in these calculations, it is not likely that more accurate calculations would significantly alter the order of estimates. Thus, we believe these results serve as strong evidence that transitions through triplet states do not have appreciable contributions for these dye molecules. For these molecules, the possibility of going through conical intersections followed by activated processes is not plausible either because activated crossing in the excited state manifold, if a rate-determining step, should be insensitive to the energy gap between excited and ground electronic states and cannot explain the experimental observation.[21]

In summary, we have conducted computational modeling and theoretical analyses of nonradiative decay rates from the first singlet excited states for two NIR/SWIR dye molecules, Flav5 and Flav7, which were shown to exhibit the energy gap law behavior. The trends of our theoretical rates are in good agreement with those of the experimental data. Theoretical data provided in Table 2 also elucidate that the difference between the decay rates of Flav5 and Flav7 come from the combination of differences in the values of NDC terms and the energy gap, with the former playing more significant role. Additional calculations for deuterated dye molecules corroborate our conclusion and indeed serve as good evidence that the cumulation of all NDC terms along all Franck−Condon modes in the excited electronic state provides the major route for the nonradiative decay of NIR/SWIR dye molecules exhibiting the energy gap law behavior. Pending future efforts for broader class of dye molecules and validation through higher level theoretical/computational studies[15,46−50] that can provide more satisfactory description of Duschinsky and non-Condon effects, anharmonic contributions, and more detailed dynamics simulation, the present work serves as a simple but essential theoretical model capable of providing semiquantitative description of the nonradiative decays of NIR/SWIR dye molecules exhibiting energy gap law behavior.

■ ASSOCIATED CONTENT

Supporting Information

The Supporting Information is available free of charge at https://pubs.acs.org/doi/10.1021/acs.jpclett.3c02629.

Additional details and results of computation, illustration of major normal modes, derivation of expressions for derivative nonadiabatic coupling, numerical results for the dependence of derivative couplings on nuclear coordinates, calculation of Duschinsky matrix elements, calculation results of nonadiabatic rates for transition to triplet states, experimental lifetime measurements, information on materials and general experimental procedure, synthetic schemes and procedure, H NMR spectra, and C NMR spectra (PDF)

Transparent Peer Review report available (PDF)

■ AUTHOR INFORMATION

Corresponding Author

Seogjoo J. Jang − *Department of Chemistry and Biochemistry, Queens College, City University of New York, New York, New York 11367, United States; Chemistry and Physics PhD programs, Graduate Center, City University of New York, New*

https://doi.org/10.1021/acs.jpclett.3c02629
J. Phys. Chem. Lett. 2024, 15, 1802−1810

York, New York 10016, United States; orcid.org/0000-0002-9975-5504; Email: seogjoo.jang@qc.cuny.edu

Authors

Pablo Ramos − *Department of Chemistry and Biochemistry, Queens College, City University of New York, New York, New York 11367, United States*

Hannah Friedman − *Department of Chemistry and Biochemistry, University of California, Los Angeles, Los Angeles, California 90095, United States;* orcid.org/0000-0003-1184-0876

Barry Y. Li − *Department of Chemistry and Biochemistry, University of California, Los Angeles, Los Angeles, California 90095, United States;* orcid.org/0000-0001-8469-6890

Cesar Garcia − *Department of Chemistry and Biochemistry, University of California, Los Angeles, Los Angeles, California 90095, United States*

Ellen Sletten − *Department of Chemistry and Biochemistry, University of California, Los Angeles, Los Angeles, California 90095, United States;* orcid.org/0000-0002-0049-7278

Justin R. Caram − *Department of Chemistry and Biochemistry, University of California, Los Angeles, Los Angeles, California 90095, United States;* orcid.org/0000-0001-5126-3829

Complete contact information is available at: https://pubs.acs.org/10.1021/acs.jpclett.3c02629

Notes

The authors declare no competing financial interest.

■ ACKNOWLEDGMENTS

S.J.J. acknowledges partial support from the National Science Foundation (CHE-1900170) during the initial stage of this project, and major support from the US Department of Energy, Office of Sciences, Office of Basic Energy Sciences (DE-SC0021413). S.J.J. also acknowledges support from Korea Institute for Advanced Study through its KIAS Scholar program. J.R.C., H.C.F., Y.I., C.G., and E.M.S. are supported by NSF Grant CHE-2204263. J.R.C. would also like to acknowledge the Cottrell foundation for support. We also thank Prof. Daniel Neuhauser (UCLA) for supporting the computational resources for some of the calculations, which also used Expanse CPU at San Diego Supercomputer Center (SDSC) through allocation CHE230099 from the Advanced Cyberinfrastructure Coordination Ecosystem: Services & Support (ACCESS) program being supported by the National Science Foundation grants (#2138259, #2138286, #2138307, #2137603, and #2138296).

■ REFERENCES

(1) Born, M.; Oppenheimer, J. R. Zur quantentheorie der molekeln. *Ann. Phys. (Berl.)* **1927**, *389*, 457−484.

(2) Jang, S. J. *Quantum Mechanics for Chemistry*; Springer Nature: New York, 2023.

(3) Baer, M. Introduction to the theory of electronic non-adiabatic coupling terms in molecular systems. *Phys. Rep.* **2002**, *358*, 75−142.

(4) Yonehara, T.; Hanasaki, K.; Takatsuka, K. Fundamental approaches to nonadiabaticity: Toward a chemical theory beyond the Born Oppenheimer paradigm. *Chem. Rev.* **2012**, *112*, 499−542.

(5) Jasper, A. W.; Zhu, C.; Nangia, S.; Truhlar, D. G. Introductory lecture: Nonadiabatic effects in chemical dynamics. *Faraday Discuss.* **2004**, *127*, 1.

(6) Chen, X.-K.; Ravva, M. K.; Li, H.; Ryno, S. M.; Brédas, J.-L. Effect of Molecular Packing and Charge Delocalization on the Nonradiative Recombination of Charge-Transfer States in Organic Solar Cells. *Adv. Ener. Mater.* **2016**, *6*, No. 1601325.

(7) Uratani, H.; Morioka, T.; Yoshikawa, T.; Nakai, H. Fast Nonadiabatic Molecular Dynamics via Spin-Flip Time-Dependent Density-Functional Tight-Binding Approach: Application to Non-radiative Relaxation of Tetraphenylethylene with Locked Aromatic Rings. *J. Chem. Theory Comput.* **2020**, *16*, 7299−7313.

(8) Tully, J. C. Perspective: Nonadiabatic dynamics theory. *J. Chem. Phys.* **2012**, *137*, No. 22A301.

(9) Song, H.; Fischer, S. A.; Zhang, Y.; Cramer, C. J.; Mukamel, S.; Govind, N.; Tretiak, S. First principles nonadiabatic excited-state molecular dynamics in NWChem. *J. Chem. Theory Comput.* **2020**, *16*, 6418−6427.

(10) Zhao, L.; Tao, Z.; Pavosevic, F.; Wildman, A.; Hammes-Schiffer, S.; Li, X. Real-time time-dependent nuclear-electronic orbital approach: Dynamics beyond the Born-Oppenheimer approximation. *J. Phys. Chem. Lett.* **2020**, *11*, 4052−4058.

(11) Curchod, B. F. E.; Rauer, C.; Marquetand, P.; González, L.; Martinez, T. GAIMSGeneralized Ab Initio Multiple Spawning for both internal conversion and intersystem crossing processes. *J. Chem. Phys.* **2016**, *144*, No. 101102.

(12) Bian, X.; Wu, Y.; Teh, H.-H.; Zhou, Z.; Chen, H.-T.; Subotnik, J. E. Modeling nonadiabatic dynamics with degenerate electronic states, intersystem crossing, and spin separation: A key goal for chemical physics. *J. Chem. Phys.* **2021**, *154*, No. 110901.

(13) Prezhdo, O. V. Modeling non-adiabatic dynamics in nanoscale and condensed matter systems. *Acc. Chem. Res.* **2021**, *54*, 4239−4249.

(14) Shu, Y.; Zhang, L.; Chen, X.; Sun, S.; Huang, Y.; Truhlar, D. G. Nonadiabatic dynamics algorithms with only potential energies and gradients: Curvature-driven coherent switching with decay of mixing and curvature-driven trajectory surface hopping. *J. Chem. Theory Comput.* **2022**, *18*, 1320−1328.

(15) Alfonso-Hernandez, L.; Athanasopoulos, S.; Tretiak, S.; Miguel, B.; Bastida, A.; Fernandez-Alberti, S. Vibrational energy redistribution during donor-acceptor electronic energy transfer: criteria to identify subsets of active normal modes. *Phys. Chem. Chem. Phys.* **2020**, *22*, 18454−18466.

(16) Ishikawa, H.; Noyes, A. W. Photosensitization by benzene vapor: Biacetyl. The triplet state of benzene. *J. Chem. Phys.* **1962**, *37*, 583−591.

(17) Laposa, J. D.; Lim, E. C.; Kellogg, R. E. Radiationless transitions and deuterium effect on fluorescence lifetimes of some aromatic hydrocarbons. *J. Chem. Phys.* **1965**, *42*, 3025−3026.

(18) Kathayat, R. S.; Yang, L.; Sattasathuchana, T.; Zoppi, L.; Baldridge, K. K.; Linden, A.; Finney, N. S. On the origins of nonradiative excited state relaxation in aryl sulfoxides relevant to fluorescent chemosensing. *J. Am. Chem. Soc.* **2016**, *138*, 15889−15895.

(19) Hare, P. M.; Crespo-Hernández, C. E.; Kohler, B. Internal conversion to the electronic ground stateoccurs via two distinct pathways for pyrimidine bases in aqueous solution. *Proc. Natl. Acad. Sci., USA* **2007**, *104*, 435−440.

(20) Izmaylov, A. F.; Mendive-Tapia, D.; Bearpark, M. J.; Robb, M. A.; Tully, J. C.; Frisch, M. J. Nonequilibrium Fermi golden rule for electronic transitions through conical intersection. *J. Chem. Phys.* **2011**, *135*, No. 234106.

(21) Friedman, H. C.; Cosco, E. D.; Atallah, T. L.; Jia, S.; Sletten, E. M.; Caram, J. R. Establishing design principles for emissive organic SWIR chromophores from energy gap laws. *Chem.* **2021**, *7*, 3359.

(22) Englman, R.; Jortner, J. The energy gap law for radationless transitions in large molecules. *Mol. Phys.* **1970**, *18*, 145−164.

(23) Jang, S. J. A simple generalization of the energy gap law for nonradiative processes. *J. Chem. Phys.* **2021**, *155*, No. 164106.

(24) Erker, C.; Basche, T. The energy gap law at work: Emission yield and rate fluctuations of single NIR emitters. *J. Am. Chem. Soc.* **2022**, *144*, 14053−14056.

(25) Thimsen, E.; Sadtler, B.; Berezin, M. Y. Shortwave-infrared (SWIR) emitters for biological imaging: a review of challenges and opportunities. *Nanophotonics* **2017**, *6*, 1043−1054.

(26) Xie, Y.; Liu, W.; Deng, W.; Wu, H.; Wang, W.; Si, Y.; Zhan, X.; Gao, C.; Chen, X.-K.; Wu, H.; et al. Bright short-wavelength infrared organic light-emitting devices. *Nat. Photon* **2022**, *16*, 752−761.

(27) Pascal, S.; David, S.; Andraud, C.; Maury, O. Near-infrared dyes for two-photon absorption in the short-wavelength infrared: strategies towards optical power limiting. *Chem. Soc. Rev.* **2021**, *50*, 6613−6658.
(28) Li, C.; Chen, G.; Zhang, Y.; Wu, F.; Wang, Q. Advanced Fluorescence Imaging Technology in the Near-Infrared-II Window for Biomedical Applications. *J. Am. Chem. Soc.* **2020**, *142*, 14789−14804.
(29) Parr, R. G.; Yang, W. *Density-Functional Theory of Atoms and Molecules*; Oxford University Press, Oxford, 1989.
(30) Dreizler, R. M.; Gross, E. K. U. *Density Functional Theory - An Approach to the Quantum Many-Body Problem*; Springer: Berlin, 1990.
(31) Engel, E.; Dreizler, R. M. *Density Functional Theory: An advanced course*; Springer, 2011.
(32) Gross, E. K. U.; Ullrich, C. A.; Gossmann, U. J. In *Density Functional Theory*; Gross, E. K. U., Ed.; Plenum Press: New York, 1995; pp 149−171.
(33) Marques, M. A. L.; Gross, E. K. U. In *A Primer in Density Functional Theory*; Fiolhais, C., Nogueira, F., Marques, M., Eds.; Springer: Berlin, 2003; pp 144−184.
(34) Yanai, T.; Tew, D. P.; Handy, N. C. A new hybrid exchange-correlation functional using the Coulomb-attenuating method (CAM-B3LYP). *Chem. Phys. Lett.* **2004**, *393*, 51−57.
(35) Higashi, M.; Kosugi, T.; Hayashi, S.; Saito, S. Theoretical study on excited states of bacteriochlorophyll a in solutions with density functional assessment. *J. Phys. Chem. B* **2014**, *118*, 10906−10918.
(36) Li, M.; Reimers, J. R.; Ford, M. J.; Kobayashi, R.; Amos, R. D. Accurate prediction of the properties of materials using the CAM-B3LYP density functional. *J. Comput. Chem.* **2021**, *42*, 1486−1497.
(37) Li, M.; Kobayashi, R.; Amos, R. D.; Ford, M. J.; Reimers, J. R. Density functionals with asymptotic-potential corrections are required for the simulation of spectroscopic properties of materials. *Chem. Sci.* **2022**, *13*, 1492−1503.
(38) Sun, J.; Remsing, R. C.; Zhang, Y.; Sun, Z.; Ruzsinszky, A.; Peng, H.; Yang, Z.; Paul, A.; Waghmare, U.; Wu, X.; et al. Accurate first-principles structures and energies of diversely bonded systems from an efficient density functional. *Nat. Chem.* **2016**, *8*, 831−836.
(39) Reimers, J. R. A practical method for the use of curvilinear coordinates in calculations of normal-mode-projected displacements and Duschinsky rotation matrices for large molecules. *J. Chem. Phys.* **2001**, *115*, 9103−9109.
(40) Jang, S. J. *Dynamics of Molecular Excitons (Nanophotonics Series)*; Elsevier: Amsterdam, 2020.
(41) Fatehi, S.; Alguire, E.; Shao, Y.; Subotnik, J. E. Analytic derivative couplings between configuration-interaction-singles states with built-in electron-translation factors for translational invariance. *J. Chem. Phys.* **2011**, *135*, No. 234105.
(42) Ou, Q.; Bellchambers, G. D.; Furche, F.; Subotnik, J. E. First-order derivative couplings between excited states from adiabatic TDDFT response theory. *J. Chem. Phys.* **2015**, *142*, No. 064114.
(43) Jang, S. Nonadiabatic quantum Liouville equation and master equations in the adiabatic basis. *J. Chem. Phys.* **2012**, *137*, No. 22A536.
(44) Chang, J.-L. A new method to calculate Franck−Condon factors of multidimensional harmonic oscillators including the Duschinsky effect. *J. Chem. Phys.* **2008**, *128*, No. 174111.
(45) Ruhoff, P. T.; Ratner, M. A. Algorithms for computing Franck-Condon overlap integrals. *Int. J. Quantum Chem.* **2000**, *77*, 383−392.
(46) Mebel, A. M.; Hayashi, M.; Liang, K. K.; Lin, S. H. Ab Initio calculations of vibronic spectra and dynamics for small polyatomic molecules: Role of Duschinsky effect. *J. Phys. Chem. A* **1999**, *103*, 10674−10690.
(47) Niu, Y.; Peng, Q.; Shuai, Z. Promoting-mode free formalism for excited state radiationless decay process with Duschinsky rotation effect. *Sci. China Ser. B-Chem.* **2008**, *51*, 1153−1158.
(48) Niu, Y.; Peng, Q.; Deng, C.; Gao, X.; Shuai, Z. Theory of excited state decays and optical spectra: Application to polyatomic molecules. *J. Phys. Chem. A* **2010**, *114*, 7817−7831.
(49) Borrelli, R.; Peluso, A. Perturbative calculation of Franck-Condon integrals: New hints for a rational implementation. *J. Chem. Phys.* **2008**, *129*, No. 064116.
(50) Wang, Y.; Ren, J.; Shuai, Z. Evaluating the anharmonicity contributions to the molecular excited internal conversion rates with finite temperature TD-DMRG. *J. Chem. Phys.* **2021**, *154*, No. 214109.
(51) Jang, S. J.; Rhee, Y. M. Fermis golden rule rate expression for transitions due to nonadiabatic derivative couplings with respect to crude adiabatic basis. Manuscript in preparation, 2023.

https://doi.org/10.1021/acs.jpclett.3c02629
J. Phys. Chem. Lett. 2024, 15, 1802−1810